Clathrate Formation and Molecular Recognition by Novel Chalcogen–Cyano Interactions in Tetracyanoquinodimethanes Fused with Thiadiazole and Selenadiazole Rings

Takanori Suzuki,[1a] Hiroshi Fujii,[1a,b] Yoshiro Yamashita,[1c] Chizuko Kabuto,[1a] Shoji Tanaka,[1c] Masako Harasawa,[1a] Toshio Mukai,[1a,d] and Tsutomu Miyashi*,[1a]

Contribution from the Department of Chemistry, Faculty of Science, Tohoku University, Aramaki, Sendai 980, Japan, and Institute for Molecular Science, Okazaki 444, Japan.
Received June 24, 1991. Revised Manuscript Received November 27, 1991

Abstract: The intermolecular contacts between chalcogen atoms and cyano lone pairs were found to stabilize the crystalline state by electrostatic interaction. This interaction is one of the sources of the directionality in crystal packing of organic molecules and causes the formation of various types of inclusion lattices in the charge-transfer (CT) crystals of **1–3**. By using highly selective formation of CT crystals with substituted aromatic hydrocarbons, particular isomers such as *p*-xylene or 2,6-dimethylnaphthalene (2,6-DMN) could be separated from the corresponding isomer mixtures. Lattice-related interaction plays a more significant role than molecular orbital interaction in the observed selectivity for para-disubstituted benzenes. However, the latter interaction is important for the recognition of 2,6-DMN from the 2,7 isomer.

Chemical bonds between sulfur and nitrogen are intriguing, as exemplified by the hypervalency in 10-S-3 sulfuranes[2] or the superconducting behavior in the $(SN)_x$ polymer.[3] Both =N–S–N= and –N=S=N– linkages are fractions of $(SN)_x$, and the latter contains tetravalent sulfur. Due to this type of resonance, 1,2,5-thiadiazole, the five-membered heterocyclic ring containing the =N–S–N= linkage, exhibits aromatic character with six π-electrons,[4] and the aromaticity of naphtho[1,8-*cd*:4,5-*c'd'*]bis-[1,2,6]thiadiazine containing =N–S–N= moieties in six-membered rings has been well examined by Haddon et al.[5] Another interesting feature of the =N–S–N= linkage is the close intermolecular contacts of S···N in crystals, which have been observed for a wide variety of compounds containing thiadiazole or thiadiazine rings;[6] substitution of Se for S shortens the intermolecular distances.[7] These contacts may be due to intermolecular electrostatic interaction between $-N^{-}-S^{+}=N-$ dipoles and/or weak intermolecular bonding involving a partial rehybridization at S with d-orbital participation.[6]

Scheme I

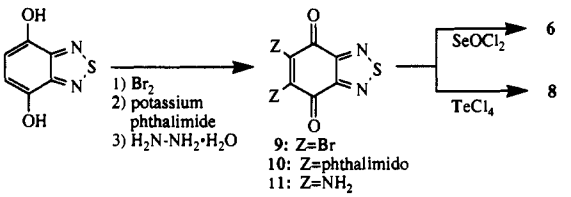

In this connection, tetracyanoquinodimethanes (TCNQs) fused with thiadiazole and selenadiazole rings are of interest because stronger intermolecular interactions are expected by larger polarization of =N–S–N= and =N–Se–N= linkages due to the delocalization of negative charge to the dicyanomethylene groups. Electrostatic interaction between the cyano group and a chalcogen atom is also expected. We previously reported the preparation of bis[1,2,5]thiadiazolotetracyanoquinodimethane (BTDA, **1**),[8] an electron acceptor, which afforded an organic metal[9] and two dimensionally conducting anion radical salts.[10] These intriguing properties might be due to a novel sulfur–cyano interaction found in the neutral crystal of **1**.[11a]

We report here a quite different aspect of chalcogen–cyano interactions in **1** and its Se analogues, that is, the formation of novel clathrate compounds. Acceptors **1–3** were found to give crystalline charge-transfer complexes (CT crystals) with aromatic hydrocarbons, and various types of inclusion lattices were formed in these crystals. Highly selective complexation followed by thermal decomplexation was applicable to the separation of a particular isomer from a mixture of isomers. A plausible mechanism for the molecular recognition is discussed on the basis of the association constant in solution and X-ray structural analyses of CT crystals.

Results

Preparation and Structure of Bis[1,2,5]chalcogenadiazolo TCNQs.[12] As described previously,[8] **1** was obtained by the

(1) (a) Tohoku University. (b) On leave from Mitsubishi Oil Co., Ltd., Research Laboratory for Development, 4-1, Ohgimachi, Kawasaki-ku, Kawasaki, 210 Japan. (c) Institute for Molecular Science. (d) Present Address: Department of Industrial Chemistry, College of Engineering, Nihon University, Tamura, Koriyama, Fukushima, 963 Japan.

(2) Lozac'h, N. *Adv. Heterocycl. Chem.* **1971**, *13*, 161. L'abbé, G.; Verhelst, G.; Vermeulen, G. *Angew. Chem., Int. Ed. Engl.* **1977**, *16*, 403. Dingwall, J. G.; McKenzie, S.; Reid, D. H. *J. Chem. Soc. C* **1968**, 2543. Perkins, C. W.; Martin, J. C.; Arduengo, A. J.; Lau, W.; Algeria, A.; Kochi, J. K. *J. Am. Chem. Soc.* **1980**, *102*, 7753. Akiba, K.; Kashiwagi, K.; Ohyama, Y.; Yamamoto, Y.; Ohkata, K. *J. Am. Chem. Soc.* **1985**, *107*, 2721. Yamamoto, Y.; Akiba, K. *J. Am. Chem. Soc.* **1984**, *106*, 2713. Akiba, K.; Kobayashi, T.; Arai, S. *J. Am. Chem. Soc.* **1979**, *101*, 5857. Matsumura, N.; Tomura, M.; Mori, O.; Tsuchiya, Y.; Yoneda, S.; Toriumi, K. *Bull. Chem. Soc. Jpn.* **1988**, *61*, 2419. Matsumura, N.; Mori, O.; Tomura, M.; Yoneda, S. *Chem. Lett.* **1989**, 39. Hordvik, A.; Julshamn, K. *Acta Chem. Scand.* **1972**, *26*, 343.

(3) Lou, L. F. *J. Appl. Phys.* **1989**, *66*, 979. Labes, M. M.; Love, P.; Nichols, L. F. *Chem. Rev.* **1979**, *79*, 1. Smith, R. D.; Wyatt, J. R.; DeCorpo, J. J.; Saalfeld, F. E.; Moran, M. J.; MacDiarmid, A. G. *J. Am. Chem. Soc.* **1977**, *99*, 1726. Cohen, M. J.; Garito, A. F.; Heeger, A. J.; MacDiarmid, A. G.; Saran, M. S.; Kleppinger, J. *J. Am. Chem. Soc.* **1976**, *98*, 3844. Mikulski, C. M.; Russo, P. J.; Saran, M. S.; MacDiarmid, A. G.; Garito, A. F.; Heeger, A. J. *J. Am. Chem. Soc.* **1975**, *97*, 6358. Greene, R. L.; Street, G. B.; Suter, L. J. *Phys. Rev. Lett.* **1975**, *34*, 577. Greene, R. L.; Grant, P. M.; Street, G. B. *Phys. Rev. Lett.* **1975**, *34*, 89. Walatka, V. V., Jr.; Labes, M. M.; Perlstein, J. H. *Phys. Rev. Lett.* **1973**, *31*, 1139.

(4) Dobyns, Sr. V.; Peirce, L. *J. Am. Chem. Soc.* **1963**, *85*, 3553. Momany, F. A.; Bonham, R. A. *J. Am. Chem. Soc.* **1964**, *86*, 162.

(5) Haddon, R. C.; Kaplan, M. L.; Marshall, J. H. *J. Am. Chem. Soc.* **1978**, *100*, 1235.

(6) Gieren, A.; Lamm, V.; Haddon, R. C.; Kaplan, M. L. *J. Am. Chem. Soc.* **1979**, *101*, 7277.

(7) Gieren, A.; Lamm, V.; Haddon, R. C.; Kaplan, M. L. *J. Am. Chem. Soc.* **1980**, *102*, 5070 and references cited therein.

(8) Yamashita, Y.; Suzuki, T.; Mukai, T.; Saito, G. *J. Chem. Soc., Chem. Commun.* **1985**, 1044.

(9) Ugawa, A.; Iwasaki, K.; Kawamoto, A.; Yakushi, K.; Yamashita, Y.; Suzuki, T. *Phys. Rev. B* **1991**, *43*, 14718.

(10) Suzuki, T.; Kabuto, C.; Yamashita, Y.; Mukai, T.; Miyashi, T.; Saito, G. *Bull. Chem. Soc. Jpn.* **1988**, *61*, 483.

(11) (a) Kabuto, C.; Suzuki, T.; Yamashita, Y.; Mukai, T. *Chem. Lett.* **1986**, 1433. (b) A reinvestigation of the structural analysis revealed that the space group of **1** is not *C*2 as described previously but *C*2/*m* with higher symmetry.

(12) Preparation and structural analyses of **2** and **3** were reported as a preliminary communication. Suzuki, T.; Kabuto, C.; Yamashita, Y.; Saito, G.; Mukai, T.; Miyashi, T. *Chem. Lett.* **1987**, 2285.

0002-7863/92/1514-3034$03.00/0

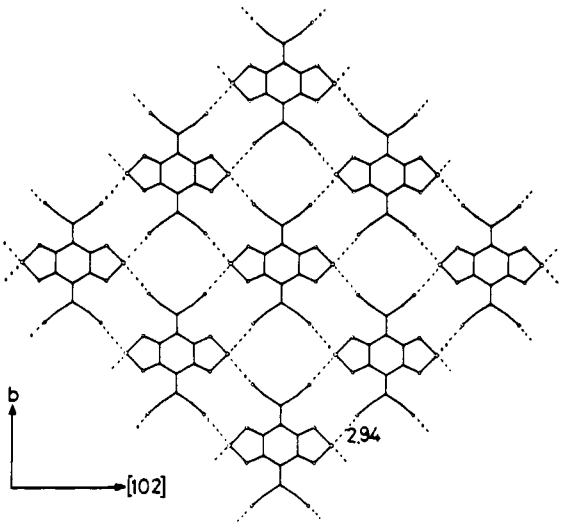

Figure 1. Coplanar sheetlike network in **3**. Se···N≡C contacts (2.94 Å) are shown by broken lines.

condensation reaction of diketone **5**[13] with malononitrile in the presence of $TiCl_4$ and dry pyridine[14] below −10 °C. Its Se analogue BSDA (**3**), prepared similarly from **7**,[13] was stable up to 400 °C, while its precursor **7** lost elemental Se on heating. The unsymmetrical acceptor, TSDA (**2**), was prepared from diketone **6**, which was derived from benzo[*c*][1,2,5]thiadiazole-4,7-diol[15] according to Scheme I. This route giving **2** could completely exclude contamination by **1** or **3**. Attempts to prepare the Te-containing acceptor **4** were unsuccessful because of the very low solubility of diketone **8** in organic solvents and facile ring opening of telluradiazole under the reaction conditions employed.

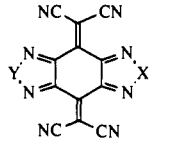

BTDA (1): X=S, Y=S
TSDA (2): X=S, Y=Se
BSDA (3): X=Se, Y=Se
TTeDA (4): X=S, Y=Te

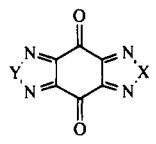

5: X=S, Y=S
6: X=S, Y=Se
7: X=Se, Y=Se
8: X=S, Y=Te

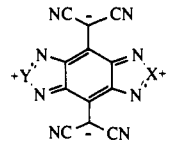

12

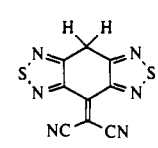

13

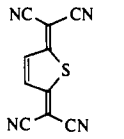

Thiophene-TCNQ (14)

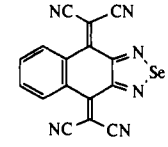

SDA-TCNNQ (15)

The X-ray structural analyses revealed that **2** and **3** crystallize isomorphously to **1**.[11b] They are planar molecules and possess a crystallographic 2-fold axis and a mirror plane along the long and short axes of the TCNQ skeleton, respectively. Short S···N≡C and/or Se···N≡C contacts in crystals connect the molecule with four neighbors, thus forming nearly coplanar "sheetlike" networks with rhombohedral linkages (Figure 1). The "sheets" stack to

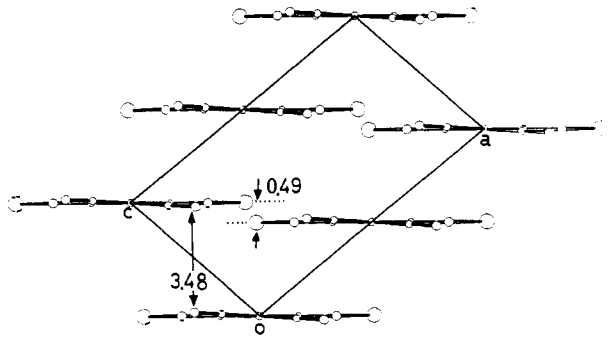

Figure 2. Sheet stacks to form infinite layers in **2** (*b* projection). The deviations between neighboring molecular planes in the sheet are 0.56, 0.49, and 0.47 Å for **1**–**3**, respectively. The interplanar distances are 3.53, 3.48, and 3.47 Å for **1**–**3**, respectively.

Table I. Comparison of Bond Lengths[a] in Neutral **1**–**3**

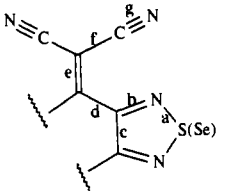

bond	1	2	3
a (X = Se)		*b*	1.790 (3)
a (X = S)	1.626 (4)	*b*	
b	1.330 (5)	1.321 (8)	1.309 (5)
c	1.421 (5)	1.433 (8)	1.453 (6)
d	1.464 (6)	1.462 (8)	1.459 (6)
e	1.351 (7)	1.361 (9)	1.367 (6)
f	1.444 (6)	1.430 (9)	1.438 (6)
g	1.126 (5)	1.135 (9)	1.132 (6)

[a] Lengths in angstroms. [b] The distance for the disordered chalcogen atom and nitrogen is 1.736 (5) Å.

form infinite layers (Figure 2) with face-to-face overlapping between heterocycles. The atomic positions of S and Se in **2** are completely disordered. The distance for S···N≡C contacts is 3.04 Å in **1**, which is 9% shorter than the sum of van der Waals (vdW) radii (S···N, 3.35 Å).[16] Stronger interactions may exist through Se···N≡C contacts because the distance for Se···N≡C in **3** (2.94 Å) is 17% shorter than the sum of vdW radii (Se···N, 3.55 Å).[16] The anion radical salt of **2** and $EtNMe_3^+$ as a counterion also crystallizes isomorphously to the $EtNMe_3^+\mathbf{1}^{\bullet-}$ salt,[10] and again shorter contacts were observed in $EtNMe_3^+\mathbf{2}^{\bullet-}$ containing Se. These results suggest that the crystal structures are identical for any CT crystal of **1**–**3** with the same donor, in which only chalcogen–cyano interactions are changed.[17] The notable difference in the molecular geometry of neutral **1**–**3** was observed in the heterocyclic moiety. Bond lengths summarized in Table I show that C=N bonds (bond b) are shortened and C–C bonds (bond c) are elongated in the order of **1**, **2**, and **3**, reflecting the smaller aromaticity of selenadiazole than thiadiazole. The elongation of exomethylene bonds (bond e) in the same order indicates a large contribution of the polarized form such as **12** for **2** and **3**. Therefore, stronger interactions in **2** and **3** could be explained by electrostatic interaction between the positive charge at chalcogen atoms and the lone pair of cyano groups.

(13) Neidlein, R.; Tran-Viet, D.; Girene, A.; Kokkinidis, M.; Wilckens, R.; Geserich, H.; Rüppel, W. *Chem. Ber.* **1982**, *115*, 2898.
(14) Aumüller, A.; Hünig, S. *Liebigs Ann. Chem.* **1984**, 618.
(15) Warren, J. D.; Lee, V. J.; Angier, R. B. *J. Heterocycl. Chem.* **1979**, *16*, 1617.
(16) Pauling, L. *The Nature of Chemical Bond*, 3rd ed.; Cornell University Press: Ithaca, NY, 1960; p 260, Tables 7–20.
(17) Several CT crystals with strong donors as well as anion radical salts of **2** showed high electrical conductivities, whose values were close to those of the corresponding CT crystals and anion radical salts of **1**, respectively (supplementary material). Because the conductivity of organic solids largely depends on the crystal structure, these results also suggest the structural similarity for any CT crystals or anion radical salts with the same donor or the same cation.

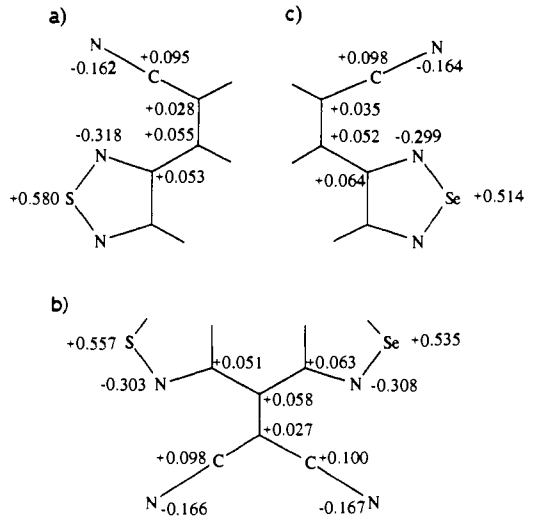

Figure 3. Total atomic charge estimated by ab initio calculations (STO-3G) based on the observed molecular geometry: (a) **1**; (b) **2**; (c) **3**.

Ab initio calculations (RHF/STO-3G)[18] of **1–3** demonstrated that large positive and negative charges localize, respectively, on chalcogen atoms and nitrogen atoms of cyano groups, suggesting polarization of =N–S–N= and/or =N–Se–N= linkages (Figure 3). This molecular polarization indicates that electrostatic stabilization is at work through the intermolecular chalcogen–cyano contacts in **1–3**. These interactions may exhibit directionality like hydrogen bonding,[19] and maximum stabilization is expected when all three atoms align linearly. The observed angles for S–N–C and/or Se–N–C atomic array in neutral **1–3** are 170.5°, 169.4°, and 169.5°, respectively. The molecular arrangement in **1–3** seems advantageous for this type of interaction because the cyano lone pair can interact to the core of S with the least repulsion of its lone pair (Figure 4b,c). These interactions will get stronger when **1–3** are negatively charged because the molecular orbital (MO) coefficients in LUMO are largely localized on the dicyanomethylene groups (Figure 4a), thus increasing the electron density on the cyano nitrogens. Contrary to our expectation, the atomic charge on Se was smaller than that on S (total atomic charge on S is +0.580 in **1** and +0.557 in **2**, and that on Se is +0.535 in **2** and +0.514 in **3**, respectively). However, polarization of =N–Se–N= linkages of **2** and **3** in molecular assembly will be larger than calculated for an isolated gaseous molecule because of the larger polarizability of Se than S. As shown in Figure 5, the electron density around Se in **2** is sparse and spread far from the core compared with that around S. It is plausible that the softness of Se can allow the closer contacts, inducing the larger polarization and stronger interaction with cyano groups in crystals.

The molecular framework of **1–3** is not the only skeleton for the appearance of chalcogen–cyano interactions. A similar sheet-type structure involved in the S···N≡C interaction was also observed for the monodicyanomethylene derivative **13** (Figure 6). Furthermore, the reported crystal structure[20] for 2,5-bis(dicyanomethylene)-2,5-dihydrothiophene (**14**) exhibited a similar coplanar arrangement and S···N≡C contacts, although these interactions were not mentioned previously because the distance for S···N≡C in **14** (3.40 Å) was nearly the same as the sum of the vdW radii. It is also noteworthy that short S···N≡C contacts between a donor and an acceptor are observed in the CT crystal of TTF·TCNQ.[21]

These observations imply that chalcogen–cyano interactions in molecular crystals play a significant role in determining the packing arrangements as do weak C–H···O hydrogen bonds[19,22] and prompt us to explore the clathrate formation of **1–3** in their CT crystals. Because low-temperature structural analysis for the molecular complex of **1** with benzene [benzene·(**1**)$_2$] revealed the formation of a unique "cage-like" network,[23] substituted benzenes and naphthalenes were chosen as electron donors in the anticipation of similar inclusion lattice formation.

CT Crystals of BTDA (1) with Alkylated Benzenes and Naphthalenes. Recrystallization of **1** from *p*-xylene (pX) afforded a 1:1 CT crystal (pX·**1**), and durene·**1** (1:1) was obtained by mixing **1** with durene in CH_2Cl_2. However, no CT crystal was formed from toluene, *o*-xylene (oX), *m*-xylene (mX), ethylbenzene (ETB), *p*-ethyltoluene, *p*-diethylbenzene (DETB) or mesitylene under similar conditions. The CT crystal formation does not depend either on the number of alkyl substituents in the benzene nucleus or on the electron-donating property, suggesting that the complexation of **1** with benzene derivatives is not usual CT complexation. On the other hand, CT crystal formation depends on the molecular symmetry of a donor. The benzene molecule in benzene·(**1**)$_2$ lies on a crystallographic 2-fold axis, and both an inversion center and a 2-fold axis perpendicular to the molecular plane exist in pX and durene, which formed CT crystals with **1**. Other donors except DETB do not have such molecular symmetries. Because the molecular symmetry is related to the shape of the donor molecule, it is suggested that the complexation of **1** is rather that of the host–guest type. No complexation with DETB can be accounted for by steric effects of ethyl substituents (vide infra), which may inhibit closer packing in its CT crystal.

Because **1** can form a CT crystal selectively with pX in a mixture of C_8H_{10} aromatic hydrocarbons and thermal decomplexation of the resulting pX·**1** crystal at 150 °C afforded pX with high purity accompanied by a quantitative recovery of **1**, this procedure can be applied to the separation of pX. Because the solubility of pX·**1** in pX is low (1.36×10^{-3} mol dm^{-3} at 20 °C), the isolated yield of the pX·**1** crystal from a hydrocarbon mixture is as high as 85–94%. The purity of pX obtained by thermal decomplexation was 92–95 wt % for pX·**1** obtained at 30 °C regardless of the pX concentration in a hydrocarbon mixture. However, the CT crystals formed at lower temperatures were highly contaminated by mX, and purity decreased to 87 and 81 wt % when complexations were carried out at 0 and −18 °C, respectively. The threshold concentration of pX to afford pX·**1** was 12.4 wt % at 30 °C and decreased as the temperature was lowered (4.2 wt % at 0 °C and 2.4 wt % at −18 °C), indicating that complexation becomes easier at lower temperatures.

The association constants (K_{CT}/dm^3 mol^{-1}) for the electron donor–acceptor (EDA) complexes of C_8H_{10}·**1** were measured in CH_2Cl_2 at 30 °C by using the Benesi–Hildebrand equation.[24] Values for oX, mX, and pX were 0.32, 0.31, and 0.30, respectively. Due to the weaker donating property,[25] that for ETB was 0.12 and smaller than those of xylene isomers under the same conditions. The K_{CT} for pX increases to 0.47 at 0 °C, which may correspond to a decrease in the threshold concentration at lower

(18) (a) The authors thank the Computer Center, Institute for Molecular Science, Okazaki National Research Institutes, for the use of a HITAC M-680H and an S-820/80 computer and the library program GAUSSIAN 86. (b) GAUSSIAN 86: Frisch, M. J.; Binkley, J. S.; Schlegel, H. B.; Raghavachari, K.; Martin, R. L.; Stewart, J. J. P.; Bobrowicz, F. W.; DeFrees, D. J.; Seeger, R.; Whiteside, R. A.; Fox, D. J.; Fluder, E. M.; Pople, J. A. Carnegie-Mellon University: Pittsburgh, PA, 1986.

(19) Berkovitch-Yellin, Y.; Leiserowitz, L. *J. Am. Chem. Soc.* **1980**, *102*, 7677. Berkovitch-Yellin, Y.; Leiserowitz, L. *J. Am. Chem. Soc.* **1982**, *104*, 4052. Murray-Rust, P.; Glusker, J. *J. Am. Chem. Soc.* **1984**, *106*, 1018. Taylor, R.; Kennard, O. *Acc. Chem. Res.* **1984**, *17*, 320. Vedani, A.; Dunitz, J. D. *J. Am. Chem. Soc.* **1985**, *107*, 7653.

(20) Aurivillius, B. *Acta Chem. Scand.* **1972**, *26*, 3612.

(21) Kistenmacher, T. J.; Phillips, T. E.; Cowan, D. O. *Acta Crystallogr. Sect. B* **1974**, *30*, 763. TTF is an abbreviation of tetrathiafulvalene.

(22) Taylor, R.; Kennard, O. *J. Am. Chem. Soc.* **1982**, *104*, 5063. Sarma, J. A. R. P.; Desiraju, G. R. *Acc. Chem. Res.* **1986**, *19*, 222. Sarma, J. A. R. P.; Desiraju, G. R. *J. Chem. Soc., Perkin Trans. 2* **1987**, 1195. Seiler, P.; Dunitz, J. D. *Helv. Chem. Acta* **1989**, *72*, 1125. Desiraju, G. R. *J. Chem. Soc., Chem. Commun.* **1989**, 179. Desiraju, G. R. *J. Chem. Soc., Chem. Commun.* **1990**, 454.

(23) Suzuki, T.; Kabuto, C.; Yamashita, Y.; Saito, G.; Mukai, T.; Miyashi, T. *J. Chem. Soc., Chem. Commun.* **1988**, 895.

(24) Benesi, H. A.; Hildebrand, J. H. *J. Am. Chem. Soc.* **1960**, *82*, 2134.

(25) Frey, J. E.; Andrews, A. M.; Ankoviac, D. G.; Beaman, D. N.; Du Pont, L. E.; Elsner, T. E.; Lang, S. R.; Zwart, M. A. O.; Seagle, R. E.; Torreano, L. A. *J. Org. Chem.* **1990**, *55*, 606.

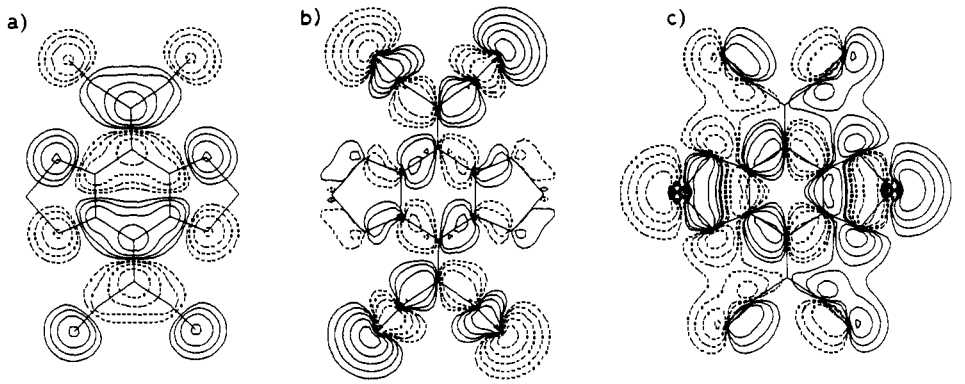

Figure 4. Contour maps of molecular orbitals (MOs) of **1**. Solid and broken lines are contours of positive and negative values, respectively, at the levels of ±0.01, ±0.02, ±0.04, ±0.08, ±0.16, ±0.32, and ±0.64. (a) LUMO ($4B_{2g}$) in a plane 1.0 au above the molecular plane. (b) 18th HOMO ($11B_{3g}$) in the molecular plane. (c) 14th HOMO ($16B_{2u}$) in the molecular plane. The latter two σ-MOs are typical ones which have a large contribution from the lone pair of cyano groups and sulfur atoms, respectively.

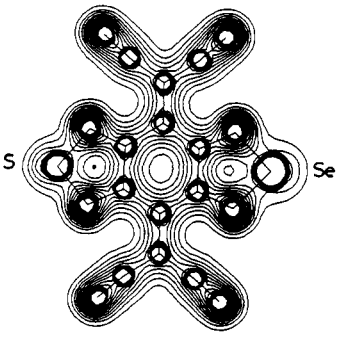

Figure 5. Contour map of the electron density in unsymmetrical acceptor **2**. Levels from 0.05 to 1.20 are fractionated by every 0.05 unit. Please note the difference around S and Se.

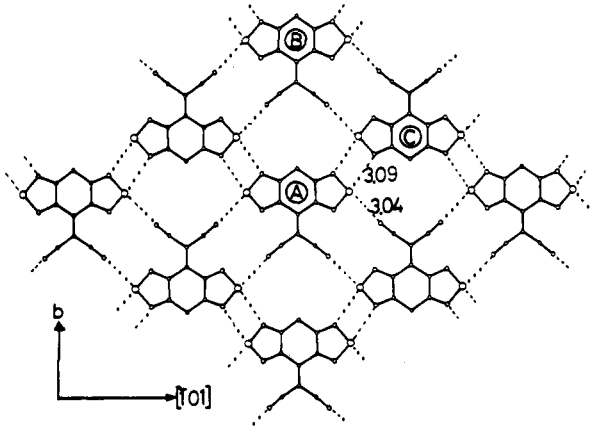

Figure 6. Coplanar sheetlike network in **13**. S···N≡C (3.04 Å) contacts are shown by broken lines. The angle of the S–N–C atomic array in S···N≡C contacts is 174.6°. The S···N contacts (3.09 Å) between heterocycles are analogous to those observed in naphthobisthiadiazines.[5-7] Molecules A and B lie on the same plane, and the deviation between neighboring molecular planes is 0.19 Å for molecules A and C or B and C.

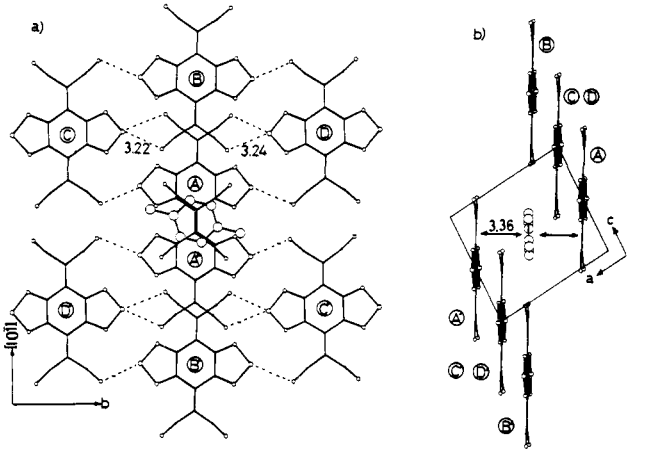

Figure 7. Cavity formation in pX·**1**: (a) top view; (b) side view. Molecules A–D and A′–D′ form corrugated sheetlike networks by S···N≡C interaction (distance, 3.22 and 3.24 Å; angle, 112.2° and 111.1°). The interplanar distance and dihedral angle between pX and molecule A (or A′) are 3.36 Å and 4.2°, respectively. The deviation of molecular planes between pX and molecule B (or B′) is 0.07 Å. Both pX and **1** exist on a center of symmetry.

temperatures. The larger K_{CT} values for oX, mX, and ETB than that for benzene (0.08 at 30 °C)[23] show that such association in solution may or may not result in CT crystal formation. Furthermore, nearly the same values for xylene isomers indicate that the recognition of xylenes by **1** is entirely absent in solution and molecular recognition occurs in the crystal-forming step due to the different thermodynamic stability of CT crystals. To investigate the factors governing the stability of the crystalline state, the X-ray analysis of pX·**1** was carried out.

The packing diagram of pX·**1** shows the existence of the sheetlike network with short S···N≡C contacts, which resembles that in neutral **1**. However, the sheet is not coplanar but corrugated along the long axis of the TCNQ skeleton, resulting in cavity formation between the two sheets, which includes a pX molecule (Figure 7). In the cavity, a pX molecule is interposed by molecules A and A′, and a large stabilization by π–π interaction is expected. The "ring–double bond"-type overlap is especially favored for CT interaction between the LUMO of **1** and the NHOMO of pX in terms of their MO coefficients. The pX molecule in the cave is also captured by the Y-shaped dicyanomethylene groups of molecules B and B′, which lie on a coplane with pX. When oX or mX gets into the cavity, the stability of the CT crystal is decreased because the transposition of the methyl groups of pX in the cavity causes unfavorable contacts with the dicyanomethylene groups of molecules B and B′ (Figure 8) and much of the CT stabilization with molecules A and A′ is lost by the parallel shifting of the benzene nucleus in the cave.

Because mX·**1** did not precipitate from neat mX even at −18 °C, high contamination by mX during the complexation of **1** with a C_8H_{10} mixture at low temperatures is not due to the concomitant crystallization of mX·**1** and pX·**1**, but is due to the coprecipitation by isomorphous replacement. Examination of the space-filling model suggests that substitution of mX for pX in the cave is possible by slight shifting and rotation of the benzene nucleus whereas oX cannot be introduced without changing the shape of the cavity, which can explain the fact that contamination is mainly caused by mX but not by oX. Although the unavailability of pure oX·**1** and mX·**1** prevented direct comparisons of their crystal structures with that of pX·**1**, both lattice-related and MO interactions seem to be most favored in the case of pX·**1**, accounting

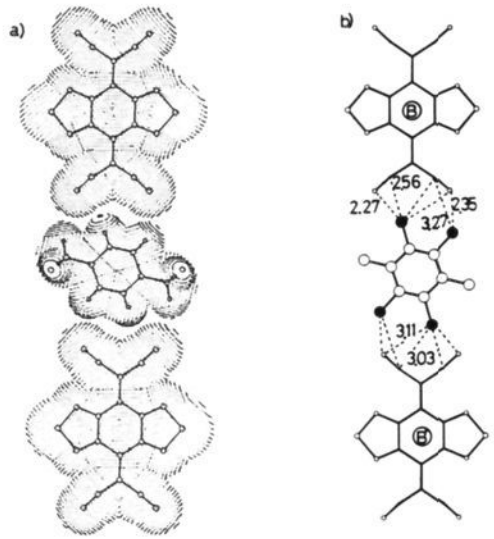

Figure 8. (a) van der Waals contacts of pX with **1** (molecules B and B'). (b) Unfavorable atomic contacts by addition of dummy methyl groups (●). Those less than 3.3 Å are shown by broken lines (sum of vdW radii: 3.55 Å for N···Me; 3.70 Å for C···Me).

for its largest stability among C_8H_{10}·**1** and selective formation.

In order to test the validity of this explanation for the selectivity, 2,6- and 2,7-dimethylnaphthalenes (DMNs), the benzo analogues of pX and mX, respectively, were chosen for further investigation. Treatment of **1** with a $C_{12}H_{12}$ isomer mixture containing an equal amount of 2,6- and 2,7-DMN (9.7 and 9.4 wt %, respectively) afforded dark brownish CT crystals in 93% yield based on **1**, and thermal decomplexation at 150–160 °C under 20 Torr gave colorless crystals composed of mainly 2,6-DMN (77.9 wt %) and 2,7-DMN (4.5 wt %). This procedure resulted in an 8-fold concentration of 2,6-DMN, whereas the concentration of 2,7-DMN was reduced to one-half of its initial value. Again, the K_{CT} values for the EDA complexes with **1** in solution were identical [5.9 dm^3 mol^{-1} for 2,6-DMN (E^{ox} +1.46 V) and 6.0 dm^3 mol^{-1} for 2,7-DMN (E^{ox} +1.52 V) at 30 °C in CH_2Cl_2]. These features are similar to the complexation of **1** with xylenes except the fact that both 2,6- and 2,7-DMN·**1** crystals could be isolated in stable form.

The structural analyses of 2,6-DMN·**1** and 2,7-DMN·**1** revealed that both crystals possess quite similar packing diagrams (Figure 9), as suggested from the comparisons of cell parameters. However, the unit cell is doubled along the *b* axis in the latter, along which unsymmetrical 2,7-DMN is aligned alternately. In both crystals, DMNs are incorporated between two coplanar "ribbon" networks of **1** by the vdW contacts and interposed from the top and the bottom by face-to-face overlapping with **1**. Although symmetrical 2,6-DMN lies in the center of the cave, 2,7-DMN is shifted to avoid unfavorable contacts of the methyl groups with **1**, resulting in the different molecular overlapping patterns (Figure 10). According to the MO consideration for these overlaps, a large CT interaction is expected between the LUMO of **1** and the NHOMO of 2,6-DMN, which may stabilize the crystalline state of 2,6-DMN·**1**. In contrast, molecular planes are slipped in the overlap of 2,7-DMN·**1**, and the stabilization by CT interaction is smaller compared with 2,6-DMN·**1**. Because lattice-related interaction is same for these crystals, MO interaction is important to explain the observed selectivity in this case.

CT Crystals of BTDA (1), TSDA (2), and BSDA (3) with Disubstituted Benzenes. To confirm the generality for selective CT crystal formation of **1**, several disubstituted benzenes containing chloro, methyl, and methoxy groups were tested. Because these derivatives have a similar molecular size to xylenes and substituents can gradually change the oxidation potential of the benzene nucleus from +1.2 to +2.3 V vs SCE, tests for complexation are informative to clarify the relationship between selectivity and CT interaction.

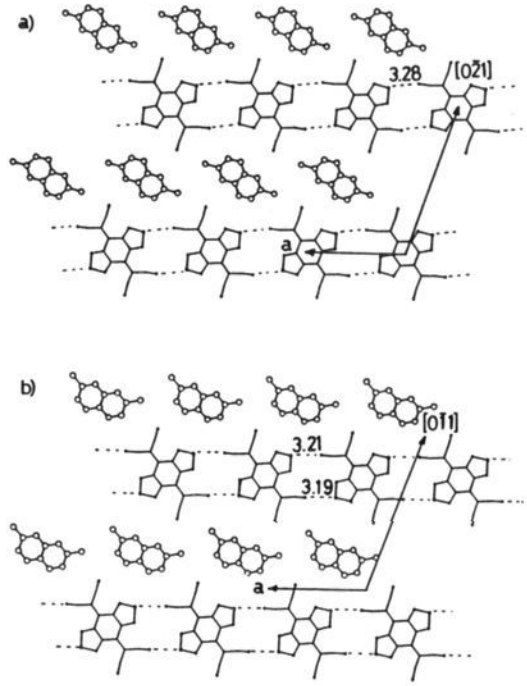

Figure 9. Coplanar ribbonlike networks of **1** incorporating DMN molecules on nearly the same plane: (a) 2,6-DMN·**1**; (b) 2,7-DMN·**1**. The deviation of neighboring molecular planes in the ribbon is 0.4 Å in the former and 0.1 Å in the latter, respectively. Distances of S···N≡C and angles of S–N–C are 3.28 Å and 161.4° in the former, and 3.21 Å, 3.19 Å, 170.6°, and 176.0° in the latter, respectively. All of the molecules exist on a center of symmetry in the former, but not in the latter.

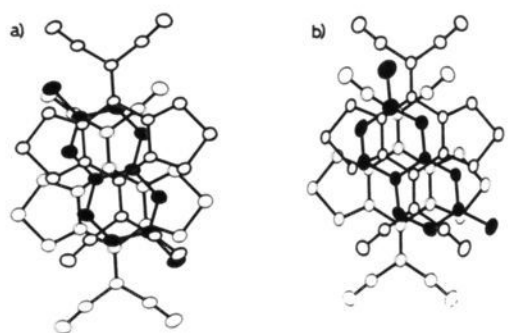

Figure 10. Molecular overlapping in 2,6-DMN·**1** (a) and 2,7-DMN·**1** (b) viewed perpendicular to the molecular plane of DMN. The interplanar distances and dihedral angles between DMN and **1** are 3.36 Å and 0.9° in the former and 3.35 Å, 3.34 Å, 1.0°, and 1.0° in the latter, respectively. Please note the slipping of molecular planes in the latter.

The results summarized in Table II show that only *p*-chlorotoluene afforded a CT crystal with **1** among its isomers. However, not only the para isomer but also the ortho isomer of chloroanisole (CA) afforded CT crystals with **1**. Moreover, all three isomers of methylanisole (MA) were found to give stable CT crystals with **1**. These results indicate that the recognition properties of **1** were concealed with an increase in CT interaction. The ease of CT crystal formation among the geometrical isomers was in the order of para, ortho, and meta. Stable CT crystal formation of oCA with **1** suggested that the oX·**1** crystal could be formed under restricted conditions. In fact, oX·**1** was isolated below 0 °C but rapidly dissociated above this temperature.

The complexations of **2** were similar to those of **1**. However, only para isomers of CA and MA afford CT crystals with **2** because **2** (E^{red} –0.12 V) is a weaker electron acceptor than **1** (E^{red} –0.02 V). Less electron donating chlorotoluenes no longer afforded CT crystals with **2**. CT interactions between **3** (E^{red} –0.23 V) and most disubstituted benzenes are not strong enough to form CT crystals. The different molar ratio of CT crystals with *o*- and

Table II. Molar Ratios[a] and Decomposition Points of CT Crystals of **1–3** and Redox Potentials[b] of Donors and Acceptors

			donor:acceptor, dec point/°C		
disubstituted benzene	isomer	E^{ox}/V	**1** (E^{red} −0.02 V)	**2** (E^{red} −0.12 V)	**3** (E^{red} −0.23 V)
chlorotoluene	*o*	+2.26			
	m	+2.25			
	p	+2.12	1:1, 90–100		
xylene (X)	*o*	+1.95	*c*		
	m	+2.07			
	p	+1.96	1:1, 120–135	1:1, 90–95	
chloroanisole (CA)	*o*	+1.81	1:1, 85–90		
	m	+1.86	*c*		
	p	+1.76	1:1, 100–105	1:1, 95–100	
methylanisole (MA)	*o*	+1.54	1:1, 110–115		
	m	+1.61	1:1, 65–75		
	p	+1.53	1:1, 110–120	1:1, 105–110	
dimethoxybenzene (DM)	*o*	+1.34	2:1, 120–130	2:1, 95–100	
	m	+1.43	2:1, 115–130	2:1, 92–95	2:1, 87–95
	p	+1.24	1:1, 200–205	1:1, 185–200	1:1, 190–200

[a] Donor to acceptor ratios, determined on the basis of elemental analyses. A blank entry denotes no crystal formation. [b] Measured by cyclic voltammetry, E/V vs SCE, 0.1 mol dm^{-3} Et_4NClO_4 in MeCN, scan rate 100 mV s^{-1}, Pt wire electrode. [c] Easy dissociation to neutral species. See the Experimental Section.

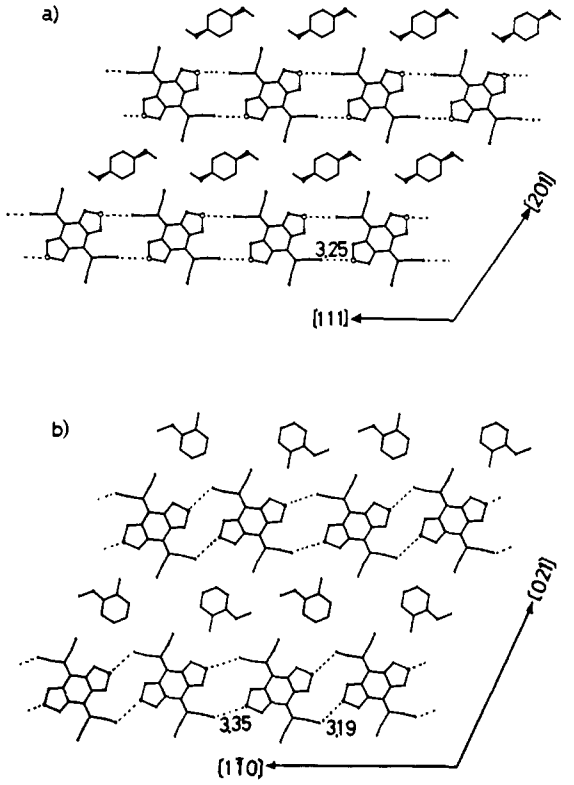

Figure 11. Coplanar arrangement of molecules in pMA·**1** (a) and oMA·**1** (b). Distances of S···N≡C and angles of S–N–C are 3.25 Å and 147.7° in the former and 3.19 Å, 3.35 Å, 120.9°, and 146.5° in the latter, respectively. All of the molecules exist on a center of symmetry in the former, but not in the latter.

m-dimethoxybenzene (2:1) indicates that these crystals possess quite different crystal structures from the others, probably because of their strong donating properties as well as the steric effects of the two methoxy substituents.

Among the disubstituted benzenes examined, complexations of MAs with **1–3** well represent the relationship between CT crystal formation and CT interaction. That is, all three isomers might form CT crystals when CT interaction is enough, but the CT crystals of the meta and ortho isomers dissociate into neutral species as CT interaction decreases, and then the formation of the CT crystal with the para isomer becomes impossible. The X-ray structural analyses of pMA·**1** and oMA·**1** revealed the important contribution of lattice-related interactions by chalcogen–cyano contacts to stabilize the crystalline state.

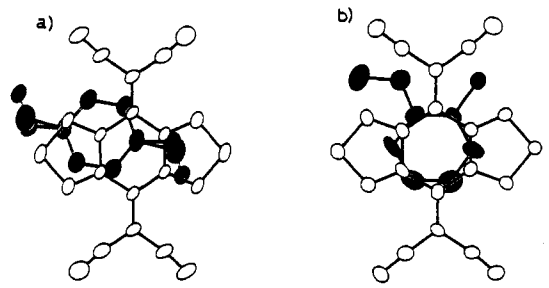

Figure 12. Molecular overlapping in pMA·**1** (a) and oMA·**1** (b). Interplanar distances and dihedral angles are 3.39 Å and 1.6° in the former and 3.36 Å and 0.1° in the latter, respectively. Two crystallographically independent overlapping patterns in the latter are coincidentally the same.

The crystal structure of pMA·**1** is different from that of pX·**1**, but resembles the 2,6-DMN·**1** crystal. Both pMA and **1** lie on a center of symmetry. Linear and coplanar "ribbon" networks of **1** are formed by S···N≡C interactions. Cavities are formed between two "ribbons" nearly on the same plane. A pMA molecule is closely packed in the center of the cave, and its substituents are completely disordered (Figure 11a). Although pMA and **1** are stacked face-to-face, overlapping in forming equally spaced mixed columns, the molecular overlap shown in Figure 12a is unfavorable for efficient CT interaction.

A similar coplanar arrangement of molecules was also observed in the oMA·**1** crystal (Figure 11b). However, in this case the "ribbon" is not linear but winds on the plane to avoid unfavorable contacts with the substituents of oMA, and large spaces are left unoccupied between the "ribbons". In contrast to the case of pMA·**1**, effective CT stabilization is expected in oMA·**1** through the interaction of the LUMO of **1** and the NHOMO of oMA by the overlap shown in Figure 12b.

The two factors are adversely operative in pMA·**1** and oMA·**1** to stabilize the crystalline state. In a pMA·**1** crystal, closer packing is accomplished by forming the compact clathrate, whereas the stabilization by S···N≡C interaction is smaller in oMA·**1** because of the nonlinearity of the S–N–C atomic array. In contrast, the molecular overlapping patterns indicate that CT stabilization in crystals is larger in the latter than in the former. Competitive complexation of **1** with an isomer mixture of MAs (1:1:1) resulted in the exclusive formation of pMA·**1** (oMA:mMA:pMA = 2:5:93). This result clearly shows that the CT crystal with pMA is thermodynamically more stable than that with oMA, so that the stabilization by clathrate formation and S···N≡C interaction is more important than CT interaction in crystals.

To investigate the steric effects of side chains on the benzene nucleus, we examined complexations with *p*-dialkoxybenzenes

which have donating properties similar to *p*-dimethoxybenzene (pDM, E^{ox} +1.23 V). Hydroquinone diethyl ether (*p*-diethoxybenzene, pDE, E^{ox} +1.23 V) formed stable 1:1 CT crystals with **1** and **2**. In contrast, pDE·**3** was not obtained. Hydroquinone dioctyl ether[26] (E^{ox} +1.19 V) containing long alkyl chains no longer formed CT crystals with **1**–**3**. These results show that the steric effects of side chains on the ease of complexation are as important as their electronic effects. This finding is in accord with results showing that only two carbon chains prevent CT crystal formation of **1** with either *p*-ethyltoluene (pET) or *p*-diethylbenzene (DETB). The stable CT crystal formation of pMA or pDM possessing a similar molecular size to pET or DETB, respectively, is due to their stronger donating properties. Thus, an increase in CT stabilization makes it possible to form CT crystals by suppressing disadvantageous steric effects. However, CT interaction does not cancel the disadvantages of steric effects but simply increases the thermodynamic stability of CT crystals, which is clearly shown from the predominant formation of pDM·**1** over pDE·**1** (68:32) in the competitive complexation of **1** with a 1:1 mixture of pDM and pDE.

Discussion

The investigations of bischalcogenadiazolo TCNQs, **1**–**3**, described above revealed that the contacts between chalcogen atoms and cyano groups stabilized the crystalline state by electrostatic interaction, and various types of inclusion lattices ("templates") such as "cage", "sheet", and "ribbon" were formed in CT crystals, which include donor–guest molecules. On the other hand, scarce complexation of a weak acceptor **3** and the existence of a threshold concentration[27] for pX·**1** formation clearly show that EDA complexation in solution is the prerequisite to form CT crystals and MO interaction between donor–guest and acceptor–host molecules is also important to stabilize the crystalline state.

Both lattice-related electrostatic interaction and MO interaction are different from crystal to crystal, changing the thermodynamic stability of the crystalline state. The advantage of stability results in the selective CT crystal formation of a particular donor over its geometrical isomers. The type of template was the same for the CT crystals of geometrical isomers (2,6-DMN·**1** and 2,7-DMN·**1**; pMA·**1** and oMA·**1**). In the case of 2,6- and 2,7-DMN possessing such similar molecular shapes that a eutectic mixture was formed, lattice-related interaction was the same because nearly the same template was formed. As predicted from the crystal structure of pX·**1**, MO interaction in 2,6-DMN·**1** was further strengthened and resulted in its predominant formation. When geometrical isomers possess different molecular shapes, such as disubstituted benzenes with different substituents shown in Table II, stabilization by lattice-related interaction changes considerably because the shape of the template must be disturbed for the same type of template to include the less favored isomers. This is the case for pMA·**1** and oMA·**1**, and comparison of their crystal structures reveals that the contribution of lattice-related interaction is more important than that of MO interaction.

In any case, particular isomers having higher molecular symmetry are favored in forming CT crystals with **1**–**3**. This phenomenon can be rationalized by considering the nature of lattice-related interaction through the chalcogen–cyano contacts. That is, electrostatic interaction in the template is maximized when the molecules connected by chalcogen–cyano contacts are related by a crystallographic symmetry, such as an inversion center, because acceptor–host molecules belong to the point group D_{2h}; less favored isomers of lower molecular symmetry make the arrangement of acceptor–host unsymmetrical, thus decreasing the stabilization of CT crystals. In other words, the cavity formed by acceptor–hosts is inherently symmetric, which is favored for the donor–guests with high symmetry but not for those with unsymmetrical shapes.

Selective CT crystal formation using chalcogen–cyano interactions is not limited to the case of **1**–**3**. Selenadiazolotetracyanonaphthoquinodimethane (SDA-TCNNQ, **15**),[28] in which one heterocyclic ring of **3** is replaced by a benzene ring, exhibited very high 2,6-DMN selectivity (97.2 wt %) upon treatment with a $C_{12}H_{12}$ mixture, and complexation of thiophene-TCNQ **14**[29] also resulted in the predominant formation of 2,6-DMN·**14** (52.1 wt %) over 2,7-DMN·**14** (2.9 wt %), showing the large value of the 2,6-DMN/2,7-DMN ratio. The recognition of 2,6-DMN over 2,7-DMN by **14** or **15** is not due to their TCNQ-type skeleton, because TCNQ itself shows only low selectivity (2,6-DMN, 13.9 wt %; 2,7-DMN, 1.7 wt %; others, 84.4 wt %) under similar conditions.

It is concluded that the interaction between chalcogen atoms and cyano groups in crystals is identified as one of the sources of the directionality in crystal packing of organic molecules. This interaction is important in designing new host molecules for lattice inclusion type complexation and is also useful in the field of solid-state reactions which require topochemical control of molecular arrangements.

Experimental Section

General. Melting points are reported uncorrected. MS spectra were obtained in the EI mode at 13.5 or 25 eV. ^{1}H NMR spectra were recorded at 200 MHz in $CDCl_3$. Gas chromatography (GC) was carried out using a 50-m capillary column of SPX-1, OV-1, or DMN267.

Preparation of 4*H*,8*H*-4,8-Bis(dicyanomethylene)benzo[1,2-*c*:4,5-*c*']bis[1,2,5]thiadiazole (BTDA, 1).[8] To a suspension of diketone **5**[13] (6.0 g, 26.8 mmol) in dry chloroform (390 mL) were added dropwise $TiCl_4$ (20.7 g, 109 mmol) at room temperature and then a dry chloroform solution (200 mL) containing malononitrile (5.13 g, 77.7 mmol) and dry pyridine (42 mL) at −50 °C over 30 min. After the mixture was stirred for 6.5 h below −10 °C, cold ether (150 mL) was added to give yellow-green precipitates, which were quickly collected and washed successively with ether, water, and warm water. The crude product (7.16 g) was fractionally recrystallized from acetone to give 6.72 g of **1** and 0.2 g of **5**. Gradient sublimation (4×10^{-2} Torr, 300 °C) of 6.17 g of **1** onto Teflon afforded 5.64 g (72%) of **1** as yellow crystals: mp 375–380 °C dec; IR (KBr) 2225 cm^{-1}; UV (MeCN) λ_{max} = 384 (log ε 4.53), 364 (4.50), 309 (4.45), 303 (4.36, sh), 246 (4.04), 239 (4.06) nm; MS *m*/*z* 320 (M^+). Anal. Calcd for $C_{12}N_8S_2$: C, 45.00; H, 0.00; N, 34.98; S, 20.02. Found: C, 45.19; H, 0.00; N, 35.16; S, 20.14.

Preparation of 4*H*,8*H*-4,8-Bis(dicyanomethylene)[1,2,5]selenadiazolo[3,4-*f*]-2,1,3-benzothiadiazole (TSDA, 2). To a suspension of diketone **6** (3.52 g, 13.0 mmol) in dry chloroform (400 mL) were added dropwise $TiCl_4$ (10 g, 52 mmol) and then a dry chloroform solution (100 mL) containing malononitrile (3.43 g, 52.0 mmol) and dry pyridine (20 mL) at 0 °C. After the mixture was stirred for 26 h at room temperature, ether (300 mL) was added at −20 °C to give insoluble precipitates, which were crystallized by triturating with ice–water. The crude product was filtered and washed with water. Recrystallization from DMF–water followed by gradient sublimation (330 °C, 4×10^{-2} Torr) gave 3.44 g (72%) of **2** as yellow cubes: mp > 400 °C; IR (KBr) 2224 cm^{-1}; UV (MeCN) λ_{max} = 367 (log ε 4.47), 327 (4.52), 248 (3.97, sh), 239 (4.06) nm; MS *m*/*z* (relative intensity) 368 (M^+, 100), 366 (M^+, 21), 80 (86), 78 (13). Anal. Calcd for $C_{12}N_8SSe$: C, 39.25; H, 0.00; N, 30.52. Found: C, 39.51; H, 0.00; N, 30.45.

Preparation of 4*H*,8*H*-4,8-Bis(dicyanomethylene)benzo[1,2-*c*:4,5-*c*']bis[1,2,5]selenadiazole (BSDA, 3). To a suspension of diketone **7**[13] (225 mg, 0.80 mmol) in dry CH_2Cl_2 (30 mL) were added $TiCl_4$ (0.76 g, 4.0 mmol) and then a dry CH_2Cl_2 solution (10 mL) containing malononitrile (240 mg, 3.63 mmol) and dry pyridine (3.2 mL), and the mixture was heated under reflux for 8 h. The resulting greenish precipitates were filtered and washed with CH_2Cl_2 and warm water. After drying in vacuo, recrystallization from DMF followed by gradient sublimation (390 °C, 4×10^{-2} Torr) gave **3** as yellow cubes (235 mg) in 71% yield: mp > 400 °C; IR (KBr) 2223 cm^{-1}; UV (MeCN) λ_{max} = 380 (log ε 4.46, sh), 351

(26) Hartley, G. S. *J. Chem. Soc.* **1939**, 1828.

(27) For the experiments to determine threshold values, the concentration of the EDA complex ([pX·**1**]/mol dm^{-3}) in the mother liquor was estimated from the pX concentration of the mother liquor, recovered weights of **1** from the mother liquor, and K_{CT} values. The values of [pX·**1**] were (1.4–1.2) × 10^{-3} at 30 °C and 1.2 × 10^{-3} at 0 °C, respectively. These values are close to the solubility of pX·**1** in pX (1.36 × 10^{-3} mol dm^{-3} at 20 °C), suggesting that the existence of thresholds is attributed to the dissolution equilibrium of pX·**1**, and the larger K_{CT} value at lower temperature can increase the concentration of the EDA complex resulting in the decrease of threshold concentration.

(28) The X-ray analysis of neutral **15** revealed that similar Se···N≡C contacts connected the molecules to form a two-dimensional network: Suzuki, T.; Kabuto, C.; Yamashita, Y.; Mukai, T. *Chem. Lett.* **1987**, 1129.

(29) Gronowitz, S.; Uppstrom, B. *Acta Chem. Scand.* **1974**, *B28*, 981.

(4.62), 242 (4.02) nm; MS *m/z* (relative intensity) 416 (M^+, 88), 414 (M^+, 97), 412 (M^+, 34), 160 (100), 158 (77), 78 (16). Anal. Calcd for $C_{12}N_8Se_2$: C, 34.81; H, 0.00; N, 27.06. Found: C, 34.98; H, 0.00; N, 27.05.

Preparation of Unsymmetrical Diketones 6 and 8. Bromine (46 g, 288 mmol) was added to a solution of benzo[*c*][1,2,5]thiadiazole-4,7-diol[15] (15.5 g, 98 mmol) in ethanol (550 mL). After stirring for 14 h at room temperature, the solution was concentrated to 150 mL to give 5,6-dibromobenzo[*c*][1,2,5]thiadiazole-4,7-dione (**9**) as yellow needles with analytical purity (28.1 g, 88%), which were recrystallized from benzene–ethanol.

A suspension of **9** (5.0 g, 15.4 mmol) and potassium phthalimide (5.88 g, 31.8 mmol) in dry DMF (100 mL) was stirred for 19 h at room temperature. After the addition of water (200 mL), separated precipitates were filtered, washed with water, and dried in vacuo. Gradient sublimation (345 °C, 4 × 10^{-2} Torr) gaved 5.19 g of 5,6-diphthalimidobenzo[*c*][1,2,5]thiadiazole-4,7-dione (**10**) as yellow crystals in 74% yield.

To a suspension of **10** (5.19 g, 11.4 mmol) in 120 mL of water was added dropwise hydrazine hydrate (80%, 30 mL) at 0 °C, and the mixture was stirred for 1 h at 0 °C and then for 1 h at room temperature. During stirring, 5,6-diaminobenzo[*c*][1,2,5]thiadiazole-4,7-dione (**11**) was separated as black-violet precipitates (1.89 g, 85%), which were collected, washed with water, and dried in vacuo.

Selenium oxychloride (8.54 g, 51.5 mmol) was added dropwise at 0 °C to a suspension of diamine **11** (2.78 g, 14.2 mmol) in dry CH_2Cl_2 (150 mL) containing dry triethylamine (10 mL), and the mixture was stirred for 30 min at 0 °C and then for 6 h at room temperature. The resulting reddish precipitates were collected, washed with MeOH, and dried in vacuo. Gradient sublimation (260 °C, 4 × 10^{-2} Torr) gave 3.65 g (95%) of 4*H*,8*H*-[1,2,5]selenadiazolo[3,4-*f*]-2,1,3-benzothiadiazole-4,8-dione (**6**) as yellow crystals.

A dry MeCN solution (10 mL) of tellurium tetrachloride (647 mg, 2.4 mmol) was added dropwise to a suspension of diamine **11** (169 mg, 1.0 mmol) in dry MeCN (20 mL) containing 10 mL of dry triethylamine. The mixture was stirred for 23 h at room temperature. Gradient sublimation (400 °C, 4 × 10^{-2} Torr) of the resulting brown solid (520 mg) gave 50 mg (16%) of 4*H*,8*H*-[1,2,5]telluradiazolo[3,4-*f*]-2,1,3-benzothiadiazole-4,8-dione (**8**) as dark brown microcrystals.

Data for **9**: mp 224–226 °C dec; IR (KBr) 1680 cm^{-1}; MS *m/z* (relative intensity) 326 (M^+, 35), 324 (M^+, 91), 322 (M^+, 27), 245 (91), 243 (100). Anal. Calcd for $C_6N_2O_2SBr_2$: C, 22.25; H, 0.00; N, 8.65. Found: C, 22.54; H, 0.07; N, 8.37. **10**: mp > 400 °C; IR (KBr) 1795, 1735, 1710 cm^{-1}; ^1H NMR δ 7.76–7.81 (2 H, m), 7.88–7.93 (2 H, m); MS *m/z* 456 (M^+). Anal. Calcd for $C_{22}H_8N_4O_2S$: C, 57.90; H, 1.77; N, 12.28. Found: C, 57.77; H, 1.68; N, 12.27. **11**: mp > 350 °C dec; IR (KBr) 3450, 3350, 3175, 1655, 1615, 1580 cm^{-1}; MS *m/z* 196 (M^+). Anal. Calcd for $C_6H_4N_4O_2S$: C, 36.76; H, 1.87; N, 28.30. Found: C, 36.74; H, 2.06; N, 28.56. **6**: mp > 400 °C; IR (KBr) 1700 cm^{-1}; MS *m/z* (relative intensity) 272 (M^+, 100), 270 (M^+, 52). Anal. Calcd for $C_6N_4O_2SSe$: C, 26.58; H, 0.00; N, 20.67. Found: C, 26.56; H, 0.00; N, 20.48. **8**: mp > 400 °C; IR (KBr) 1691 cm^{-1}; MS *m/z* (relative intensity) 322 (M^+, 58), 320 (M^+, 52), 318 (M^+, 33), 166 (100). Anal. Calcd for $C_6N_4O_2STe$: C, 22.54; H, 0.00; N, 17.52. Found: C, 22.08; H, 0.00; N, 17.21.

Preparation of 4*H*,8*H*-4-(Dicyanomethylene)benzo[1,2-*c*:4,5-*c*']bis[1,2,5]thiadiazole (13). A suspension of 4,8-bis(dicyanomethyl)benzo[1,2-*c*:4,5-*c*']bis[1,2,5]thiadiazole (dihydro-**1**)[30] (120 mg, 0.37 mmol) in 60 mL of MeOH and 4 mL of hydrochloric acid was heated under reflux for 7 h. Concentration of solvent gave **13** as colorless needles (70 mg) in 73% yield: mp 234–237 °C dec; IR (KBr) 2218 cm^{-1}; ^1H NMR δ 4.72 (s); MS *m/z* (relative intensity) 258 (M^+, 100), 231 (33). Anal. Calcd for $C_9H_2N_6S_2$: C, 41.85; H, 0.78; N, 32.54; S, 24.83. Found: C, 42.14; H, 0.62; N, 32.38; S, 24.62.

Preparation of $EtNMe_3^+2^{\cdot-}$ Salt. Finely powdered **2** (50 mg, 0.136 mmol) was well suspended in dry acetonitrile (30 mL) containing trimethylethylammonium methylsulfate (0.016 mol dm^{-3}) as a supporting electrolyte. By using a controlled potential electrolyzer, electrochemical reduction at −0.32 V vs SCE for 4 h gave $EtNMe_3^+2^{\cdot-}$ as black powder: mp 250–251 °C; IR (KBr) 2167 cm^{-1}. Anal. Calcd for $C_{17}H_{14}N_9SSe$: C, 44.84; H, 3.10; N, 27.68. Found: C, 44.90; H, 3.18; N, 27.68.

Preparation of CT Crystals of BTDA (1) with Alkylated Benzenes and Naphthalenes. pX·**1** was obtained as red plates or powder by recrystallizing **1** from pX or simply by mixing **1** and pX at room temperature for 1 min. Durene·**1** was prepared by mixing **1** and durene in CH_2Cl_2. 2,6-DMN·**1** was obtained as dark violet needles by mixing 2,6-DMN and **1** in CH_2Cl_2, and 2,7-DMN·**1** was also obtained by a similar direct method in CH_3CN as dark violet needles.

pX·**1**: mp 120–135 °C dec; IR (KBr) 2214 cm^{-1}. Anal. Calcd for $C_{20}H_{10}N_8S_2$ (1:1): C, 56.33; H, 2.36; N, 26.27. Found: C, 56.11; H, 2.15; N, 26.67. **Durene·1**: mp 180–190 °C dec, IR (KBr) 2223 cm^{-1}. Anal. Calcd for $C_{22}H_{14}N_8S_2$ (1:1): C, 58.14; H, 3.10; N, 24.65. Found: C, 57.98; H, 2.90; N, 24.64. **2,6-DMN·1**: mp 210–245 °C dec; IR (KBr) 2223 cm^{-1}. Anal. Calcd for $C_{24}H_{12}N_8S_2$ (1:1): C, 60.49; H, 2.54; N, 23.51. Found: C, 60.59; H, 2.32; N, 23.54. **2,7-DMN·1**: mp 215–235 °C dec; IR (KBr) 2222 cm^{-1}. Anal. Calcd for $C_{24}H_{12}N_8S_2$ (1:1): C, 60.49; H, 2.54; N, 23.51. Found: C, 60.74; H, 2.36; N, 23.47.

Determination of Association Constants (K_{CT}). In the presence of a large excess of donor, K_{CT} values for the EDA complexes of **1** were determined photospectroscopically in CH_2Cl_2 at 30 °C using the Benesi–Hildebrand equation.[24] The K_{CT} value for pX·**1** was also measured at 0 °C. In all cases, linear correlations (γ = 0.998–0.999, n = 5–8) were observed, indicating a 1:1 molar ratio for the EDA complexes. In the case of benzene derivatives the CT absorption band appeared as the elongated end absorptions. Molar absorption coefficients (ϵ/dm^3 mol^{-1} cm^{-1}) for the EDA complexes are as follows: oX·**1**, 3700 at 460 nm; mX·**1**, 3700 at 460 nm; pX·**1**, 3600 at 460 nm; ETB·**1**, 2700 at 460 nm. The CT absorption spectrum of 2,6-DMN·**1** of 2,7-DMN·**1** possessed two maxima[31] corresponding to the transitions for NHOMO (DMN) to LUMO (**1**) and HOMO (DMN) to LUMO (**1**), which appeared at 450 and 555 nm for 2,6-DMN·**1** (ϵ/dm^3 mol^{-1} cm^{-1}: 2100 at 480 nm) or at 450 and 550 nm for 2,7-DMN·**1** (ϵ/dm^3 mol^{-1} cm^{-1}: 2200 at 480 nm). In these measurements, the concentration of **1** is (1.77–2.52) × 10^{-4} mol dm^{-3}, those for benzenes are 0.269–2.76 mol dm^{-3}, and those for DMNs are (4.04 × 10^{-2})–0.257 mol dm^{-3}.

Separation of pX by Selective CT Crystal Formation with BTDA (1). Finely powdered **1** (500 mg, 1.56 mmol) was suspended in 25 g of a C_8H_{10} mixture (oX:mX:*pX*:ETB = 22.4:41.7:*20.0*:15.9 wt %) and stirred for 2 h at 30 °C. The color of the suspension gradually turned from yellow to red, and the resulting CT crystals were filtered and dried in vacuo (4 × 10^{-2} Torr) for 3 h at room temperature (570 mg, yield 86%). The yield of CT crystals did not change with prolonged stirring, and the yields were 84%, 85%, and 87% for the reaction times of 45 min, 4 h, and 14.5 h, respectively. Decomplexation of the CT crystals (556 mg, 1.31 mmol) at 150 °C under ambient pressure using a Kugelrohr glass tube oven afforded a colorless oil (109 mg, 1.03 mmol) and **1** (432 mg, 1.32 mmol). GC analysis of the resulting oil showed that it was composed of 93.4 wt % of pX and a small amount of other isomers (oX, 0.72 wt %; mX, 5.39 wt %; ETB, 0.46 wt %), and the composition did not depend on the reaction time for complexation.

Determination of Threshold Concentration of pX To Afford pX·1. The complexation–decomplexation experiments were carried out, changing the relative amount of mixture oil. To each 3.0 g of a C_8H_{10} mixture (oX:mX:*pX*:ETB = 22.5:42.0:*19.4*:16.0 wt %) containing 5.49 mmol of pX were added separately 401 mg (1.25 mmol), 801 mg (2.50 mmol), and 1200 mg (3.75 mmol) of powdered **1**, and the mixtures were stirred for 22–24 h at 30 °C. Filtration gave reddish crystals that weighed 501 (yield 94%), 984, and 1364 mg, respectively. Decomplexation of the CT crystals afforded pX with high purity in three cases (95.4, 94.2, and 93.9 wt %, respectively). However, the molar ratios, pX (in CT crystals): **1**, were 0.981, 0.878, and 0.591, respectively, much smaller than the ideal value (1.00) in the latter two cases. GC analyses of the mother liquors showed that the pX concentration in the latter two cases were the same, 12.4 wt %, whereas that in the first case was 15.3 wt %. These results indicate that the initial complexation stopped at the point when the pX concentration reached 12.4 wt % (the threshold value at 30 °C), even though enough pX remained in the mixture oil to perform a 1:1 complexation. These observations were reproducible for another run of similar experiments.

The thresholds at 0 °C (4.2 wt %) and −18 °C (2.4 wt %) were determined in the same manner. The isomer distributions in the oils obtained by decomplexation were as follows: oX:mX:*pX*:ETB = 0.58:11.39:*87.17*:0.86 wt % at 0 °C; 2.39:15.40:*81.04*:1.17 wt % at −18 °C.

Separation of 2,6-DMN by Selective CT Crystal Formation with BTDA (1). Finely powdered **1** (1.03 g, 3.22 mmol) was suspended in 17.22 g of a $C_{12}H_{12}$ mixture (2,6-DMN, 9.7 wt %, 2,7-DMN 9.4 wt %; 1,3- and 1,7-DMN, 25.8 wt %; 1,6-DMN, 9.6 wt %; 1,4- and 2,3-DMN, 6.6 wt %; and other small fractions) and stirred for 5.5 h at 19 °C. The resulting brown crystals were filtered, washed with *n*-hexane (5 mL × 5), and dried in vacuo (4 × 10^{-2} Torr) for 3 h (1.42 g, yield 93%).

(30) Yamashita, Y.; Suzuki, T.; Mukai, T. *J. Chem. Soc., Chem. Commun.* **1987**, 1184.

(31) (a) The energy difference between the first and second bands (0.52 eV for 2,6-DMN and 0.50 eV for 2,7-DMN) is in good agreement with the energy gap of the HOMO–NHOMO levels of 2,6-DMN (0.50 eV) estimated by MNDO calculation. (b) MNDO: Dewar, M. J. S.; Thiel, W. *J. Am. Chem. Soc.* **1977**, *99*, 4899.

Decomplexation of the CT crystal (193 mg, 0.405 mmol) at 150–160 °C under 20 Torr using a glass tube oven afforded a colorless solid (62 mg, 0.397 mmol) and **1** (128 mg, 0.401 mmol). GC analysis of the colorless solid showed that it contained 77.9 wt % of 2,6-DMN, a small amount of 2,7-DMN (4.5 wt %), and other isomers (1,3- and 1,7-DMN, 6.8 wt %; 1,6-DMN, 2.4 wt %; 1,4- and 2,3-DMN, 2.1 wt %).

Complexation of BTDA (1), TSDA (2), and BSDA (3) with Disubstituted Benzenes. CT crystals of **1–3** shown in Table II were obtained by suspending a powdered acceptor (30 mg, 0.09–0.07 mmol) in 3 mL of benzene derivatives for 10 min to 72 h at room temperature. The color of the solid changed gradually from yellow to red, violet, green, or blue depending on the donating property of the benzene. The resulting CT crystals were filtered by suction and dried in vacuo at room temperature. In some cases, prolonged drying caused decomposition of CT crystals to lose volatile donors. In the case of solid donors, CH_2Cl_2 and CH_3CN were used as solvents. The CN stretching frequencies and analytical values for CT crystals were deposited as supplementary material.

Although mCA·**1** (mp 60–65 °C dec) was obtained in a similar manner, it could not be fully characterized because of its remarkable efflorescence. Although oX·**1** could not be obtained by suspending **1** in neat oX at room temperature, its formation at 0 °C was confirmed when **1** (501 mg, 1.56 mmol) was suspended in 20 g of oX at 0 °C. After the mixture was stirred for 24 h, fine reddish needles were formed and filtered at 0 °C. This material effloresced rapidly at room temperature and lost oX in a few minutes giving neutral **1**. Drying of red crystals in vacuo for 3 h at 0 °C also caused the color change and formed an orange powder (501 mg, yield 75%, mp <70 °C dec). Thermal decomplexation of 478 mg of the orange powder in a glass tube oven at 155 °C gave 365 mg (1.14 mmol) of **1** and 103 mg (0.97 mmol) of oX, showing that the orange powder is 1:1 CT crystal of oX.

Competitive Complexation of Methylanisoles (MAs) with BTDA (1). Powdered **1** (450 mg, 1.41 mmol) was suspended in 2.00 g of an MA isomer mixture (1:1:1) and stirred for 24 h at 30 °C. The resulting reddish-violet precipitates were filtered and dried in vacuo for 3 h (553 mg, yield 89%, mp 100–120 °C dec). Thermal decomplexation (130 °C, 18 Torr) of the CT crystal (537 mg, 1.22 mmol) gave a faintly orange oil (136 mg, 1.12 mmol) and **1** (386 mg, 1.21 mmol). ^1H NMR analysis of the resulting oil showed that it was composed of mainly pMA (93%) with trace amounts of oMA (2%) and mMA (5%). Similar experiments were carried out by using 300 mg and 150 mg of **1** under the same conditions, and the composition of the resulting oil was identical, but the yields of CT crystals were low (88% and 69%, respectively) because of the high solubility of CT crystals in an MA mixture.

Competitive Complexation of *p*-Dimethoxybenzene (pDM) and *p*-Diethoxybenzene (pDE) with BTDA (1). Powdered **1** (300 mg, 0.938 mmol) was added to a toluene solution (5 mL) of pDM (1294 mg, 9.38 mmol) and pDE (1556 mg, 9.37 mmol) (each 10 equiv) and stirred for 18 h at 30 °C. Filtration gave a brown-violet powder which was washed with toluene (1 mL × 2) and dried in vacuo for 5 h (415 mg, yield 95%). Its decomposition point is 156–157 °C, which is higher than that of pDE·**1** (126–127 °C). Thermal decomplexation (170 °C, 18 Torr) of the CT crystal (362 mg) afforded colorless crystals (113 mg) and **1** (250 mg). The ratio pDM:pDE was determined to be 68:32 on the basis of the ^1H NMR spectrum. From this value, the donor:**1** ratio in the CT crystal was proved to be 1.01. Similar results were obtained when 15 or 20 equiv each of donors in 5 mL of toluene was used. The yields of CT crystals were 93% and 95%, respectively, and the ratio pDM:pDE was 66:34 for these two cases.

Separation of 2,6-DMN by Selective CT Crystal Formation with SDA-TCNNQ (15). Finely powdered **15**[28] (83.0 mg, 0.231 mmol) was suspended in 1.23 g of a $C_{12}H_{12}$ mixture (2,6-DMN, 9.7 wt %; 2,7-DMN, 9.4 wt %) and stirred for 78 h at room temperature. Reddish-brown CT crystals were filtered, washed with ethanol (0.5 mL × 2), and dried in vacuo (4×10^{-2} Torr) for 3 h (83 mg, mp 203–204 °C dec). Thermal decomplexation of the CT crystal (145 °C, 14 Torr) gave a colorless solid (11.7 mg) and **15** (72 mg). GC analysis of a colorless solid showed that it is fairly pure 2,6-DMN (97.2 wt %) containing a small amount of 2,7-DMN (1.1 wt %) and other isomers.

Complexation of Thiophene-TCNQ (14) with a $C_{12}H_{12}$ Mixture. Finely powdered **14**[29] (71.2 mg, 0.339 mmol) was suspended in 1.61 g of a $C_{12}H_{12}$ mixture (2,6-DMN, 9.7 wt %; 2,7-DMN, 9.4 wt %) and stirred for 24.5 h at 16 °C. Dark violet precipitates were filtered, washed with *n*-hexane (1 mL × 2), and dried in vacuo (4×10^{-2} Torr) for 3 h (21 mg, mp 100–104 °C). Thermal decomplexation (80–95 °C, 19 Torr) of the CT crystal (10.8 mg) gave a colorless solid (3.1 mg) and 6.8 mg of **14**. GC analysis showed that it was composed of 52.1 wt % of 2,6-DMN, 2.9 wt % of 2,7-DMN, and other isomers.

Measurement of Redox Potentials. Reduction potentials (E^{red}) of **1–3** and oxidation potentials (E^{ox}) of donors were measured by cyclic voltammetry in CH_3CN dried over P_2O_5 and CaH_2 several times. Acceptors

Table III. Details of X-ray Structural Analyses

compd	1[a]	2	3	$EtNMe_3^+I^{-}$[b]	$EtNMe_3^+I^{2-}$	13	benzene-$(1)_2$[c]	pX·1	2,6-DMN·1	2,7-DMN·1	pMA·1	oMA·1
formula	$C_{12}N_8S_2$	$C_{12}N_8SSe$	$C_{12}N_8Se_2$	$C_{17}H_{14}N_8SSe$	$C_{17}H_{14}N_8S_2$	$C_9H_2N_6S_2$	$C_{30}H_6N_{16}S_4$	$C_{20}H_{10}N_8S_2$	$C_{24}H_{12}N_8S_2$	$C_{24}H_{12}N_8S_2$	$C_{20}H_{10}N_8S_2O$	$C_{20}H_{10}N_8S_2O$
fw	320.32	367.21	414.11	455.39	408.61	258.29	718.75	426.48	476.54	476.54	442.48	442.28
space group	$C2/m$	$C2/m$	$C2/m$	$P2_1/m$	$P2_1/m$	$C2/c$	$C2/c$	$P2_1/c$	$P\bar{1}$	$P\bar{1}$	$P\bar{1}$	$P\bar{1}$
a (Å)	8.999 (1)	9.089 (1)	9.203 (1)	15.840 (1)	15.854 (1)	9.791 (4)	29.703 (2)	8.135 (1)	10.267 (1)	10.272 (1)	8.368 (1)	17.540 (4)
b (Å)	13.056 (1)	13.226 (1)	13.388 (1)	6.491 (1)	6.482 (1)	10.345 (2)	6.666 (1)	16.100 (2)	8.322 (1)	16.704 (2)	9.184 (1)	9.358 (2)
c (Å)	5.535 (1)	5.418 (1)	5.314 (1)	9.151 (1)	9.141 (1)	10.374 (2)	15.637 (1)	7.410 (1)	7.209 (1)	7.069 (1)	7.308 (1)	6.718 (1)
α (deg)	90.0	90.0	90.0	90.0	90.0	90.0	90.0	90.0	78.19 (1)	81.08 (1)	103.69 (1)	110.72 (1)
β (deg)	99.15 (2)	98.89 (1)	98.53 (1)	99.89 (1)	100.07 (1)	99.12 (3)	108.01 (1)	97.71 (1)	102.43 (1)	96.32 (1)	96.32 (1)	98.94 (2)
γ (deg)	90.0	90.0	90.0	90.0	90.0	90.0	90.0	90.0	115.20 (1)	113.75 (1)	111.51 (1)	85.79 (2)
V (Å^3)	642.1 (2)	643.5 (2)	647.5 (2)	927.0 (1)	924.9 (2)	1037.5 (6)	2944.6 (3)	961.7 (4)	539.8 (1)	1095.3 (2)	495.5 (1)	1018.7 (4)
Z	2	2	2	2	2	4	4	2	1	2	1	2
ρ_{calcd} (g cm^{-3})	1.66	1.90	2.12	1.63	1.47	1.65	1.62	1.47	1.47	1.45	1.48	1.44
cryst dimns (mm)	0.2 × 0.2 × 0.3	0.15 × 0.2 × 0.25	0.1 × 0.1 × 0.4	0.05 × 0.15 × 0.3	0.08 × 0.15 × 0.15	0.05 × 0.1 × 0.1	0.15 × 0.25 × 0.25	0.2 × 0.25 × 0.3	0.08 × 0.1 × 0.3	0.15 × 0.2 × 0.3	0.15 × 0.25 × 0.35	0.05 × 0.1 × 0.15
abs coeff (cm^{-1})	37.980 (Cu Kα)	30.492 (Mo Kα)	56.589 (Mo Kα)	21.341 (Mo Kα)	27.653 (Cu Kα)	4.752 (Mo Kα)	3.624 (Mo Kα)	26.769 (Cu Kα)	2.659 (Mo Kα)	2.621 (Mo Kα)	2.870 (Mo Kα)	25.848 (Cu Kα)
$2\theta_{max}$ (deg)	126	65	60	60	128	55	55	126	60	60	59	105
total data measd	536	2312	1886	2920	1979	1196	3410	1555	2757	6271	2394	2571
obsd unique data	528 (non-zero)	1014 (3σ)	1649 (3σ)	2212 (1.5σ)	1596 (1.5σ)	557 (3σ)	2766 (3σ)	1421 (3σ)	1931 (3σ)	3721 (3σ)	2054 (non-zero)	1297 (3σ)
R	0.048	0.083	0.044	0.074	0.049	0.066	0.043	0.069	0.056	0.080	0.096	0.095

[a] Reference 11b. [b] Reference 10. [c] Measured at −60 °C; ref 23.

underwent multistage reversible reduction, and only the first reduction potentials were shown. Voltammograms of donors except pDM showed irreversible or quasi-reversible waves, so that half-wave potentials were estimated from the anodic peak potentials (E^{pa}) as $E^{ox} = E^{pa} - 0.03$ V. All of the values shown in the text are E/V vs SCE and were measured under the same conditions described in Table II.

X-ray Structural Analyses. All of the data collections were performed on an AFC-5R automated four-circle diffractometer equipped with a rotating anode at 13 °C unless indicated otherwise. Details are summarized in Table III. These structures were solved by direct methods using the RANTAN81 program[32] with some modification. Atomic parameters were refined by the block-diagonal least-squares method applying anisotropic temperature factors for non-hydrogen atoms. At the final stage, hydrogen atoms, if any, were included in the refinement with isotropic temperature factors. All of the calculations were carried out on an ACOS 1000 and ACOS 2020 computer at Tohoku University by using the applied library program of the UNICS III system.[33] Details of X-ray structural analyses, final atomic coordinates and thermal parameters, bond distances and angles, structure factors, and thermal ellipsoids with atom numbering systems are deposited as supplementary material.

The structural analysis of **BTDA (1)** was reinvestigated on newly collected reflection data. The space group is not $C2$ as described previously[11a] but is $C2/m$. An empirical absorption correction (Ψ-scan) was applied because of the large absorption coefficient.

TSDA (2) crystallizes isomorphously to **1**, and the chalcogen atoms are completely disordered. Two different sets of independent data were collected for accurate structural analysis, and the averaged values were used in the refinement. The structure reported previously[12] was further refined by using the hypothetical atom possessing the averaged scattering factors[34] of S and Se for the disordered chalcogen atoms. This refinement gave more satisfactory results than the constrained refinement in which the disordered chalcogen was divided into different positions for S and Se. However, the geometry of **2** at the latter refinement was used in ab initio calculations.

The estimated standard deviations (esd) for bond lengths are relatively large (0.005–0.009 Å), and the large R value may be due to some systematic errors in the data. The distance for the interatomic contacts between the disordered chalcogens and cyano groups is 2.96 Å.

BSDA (3)[12] is isomorphous to **1** and **2**. Due to the large absorption coefficient, an absorption correction was applied for the two different sets of independent data, and the whole was used in the refinement.

$EtNMe_3^+2^{\cdot-}$ salt suitable for the structural analysis was obtained as a black needlelike crystal by electrochemical reduction of **2** applying a constant current of 10 μA on a Pt wire electrode. This salt exhibited good electrical conductivity along the b axis (resistivity ρ 80 Ω cm at 295 K) with activation energy of 0.15 eV.[35]

This salt crystallizes isomorphously to the corresponding salt of **1**,[10] and the positions of S and Se are disordered. The hypothetical atom possessing the averaged scattering factor of S and Se was used in the refinement. Similar to $EtNMe_3^+1^{\cdot-}$, equally spaced (3.25 Å) "zig-zag" columns with ring–double bond-type overlapping were formed along the b axis. Molecules are connected by several chalcogen–cyano interactions and further by chalcogen–N interactions between heterocycles to form coplanar ribbon networks on the crystallographic mirror plane at y/b = 1/4 and 3/4. The distances for the disordered chalcogen–cyano contacts are 3.17 and 3.03 Å, which are shorter than those in $EtNMe_3^+1^{\cdot-}$ (3.25 and 3.12 Å). The distance for the contacts between heterocycles is 3.28 Å, also shorter than that in $EtNMe_3^+1^{\cdot-}$ (3.37 Å).

Non-hydrogen atoms of the ammonium ion appeared on the D-map. Several hydrogen atoms were also picked up from the D-map and others were calculated geometrically. The nitrogen atom and one methyl carbon of the ammonium ion exist on the mirror plane, two methyl groups are related by a mirror symmetry, and the ethyl group is orientationally disordered. Due to the disorder of heavy atoms and the ammonium ion, the esd for bond lengths are relatively large (0.005–0.010 Å for **2**), which prevents the comparisons of bond lengths with those of neutral **2**.

4*H*,8*H*-4-(Dicyanomethylene)benzo[1,2-*c*:4,5-*c*']bis[1,2,5]thiadiazole (13) used for the data collection was a slightly twinning crystal. Reflection data were collected at 25 °C, and the structure was solved by using the MULTAN78 program. The positions of hydrogen atoms were calculated geometrically.

It is a planar molecule with C_{2v} symmetry. Carbon atoms of exomethylene and the methano bridge lie on a crystallographic 2-fold axis. Coplanar sheetlike networks are stacked along the c axis forming an infinite layer structure like **1–3**.

pX·1 was obtained as single red crystals by recrystallizing **1** from CH_2Cl_2–pX. No degradation of the crystal was indicated during the data collection. Both **1** and pX are related by a center of symmetry. Ring protons were found by the D-Fourier method, and methyl protons were calculated geometrically. The geometry of **1** in this crystal is similar to that in neutral **1**.

The positions of dummy methyl groups shown in Figure 8b were calculated on the same plane of the benzene nucleus by supposing the ideal bond angle and observed bond distance (1.505 Å).

2,6-DMN·1 suitable for crystallographic work was obtained as dark violet needles from CH_2Cl_2 by slow evaporation of the solvent. Both **1** and 2,6-DMN lie on a center of symmetry and form mixed columnar stacks along the c axis.

2,7-DMN·1 was obtained as dark violet needles from CH_3CN. This complex crystallizes nearly isomorphous to 2,6-DMN·**1**, but the unit cell is doubled along the b axis. Although each of the molecules does not locate on a crystallographic center of symmetry, molecules of **1** exist on a pseudo center of symmetry such as 1/2, 1/4, 1/2. 2,7-DMN is aligned in an orderly manner along the b axis in head-to-head and tail-to-tail orientations alternately, and no transposition of methyl groups was observed.

pMA·1 lost volatile pMA gradually on standing so that the crystal was sealed in a glass capillary with pMA. Data collection was carried out at 25 °C. Each of the molecules locates on a center of symmetry. The positions of methyl and methoxy groups in pMA were completely disordered and were carefully determined from the E-map. Ring protons and several methyl protons were picked up from the D-map and others were calculated geometrically. The large R value may be due to the disorder of the substituents of pMA.

oMA·1 showed a strong tendency to effloresce and was also sealed in a glass capillary. Because of the instability and low quality of the crystal, observed data ($|F_o| > 3\sigma|F_o|$) are only one-half of those measured and the final R value is very large. No positional disorder of substituents was observed. Several hydrogen atoms were located on the D-map and others were calculated geometrically.

Acknowledgment. This work was supported by the Joint Studies Program (1989–1991) of the Institute for Molecular Science. Financial support by the Nissan Science Foundation (to T.S.) and by the Izumi Science and Technology Foundation (to T.M.) is gratefully acknowledged.

Registry No. 1, 99794-32-8; $1^{\cdot-}$·$EtNMe_3^+$, 115432-31-0; **1**·benzene, 116925-57-6; **1**·*p*X, 124591-80-6; **1**·2,6-DMN, 139346-68-2; **1**·2,7-DMN, 139346-69-3; **1**·*p*MA, 139346-70-6; **1**·*o*MA, 139346-71-7; **1**·ClC_6H_4-*p*-Me, 139346-72-8; **1**·*o*X, 139346-73-9; **1**·*o*CA, 139346-75-1; **1**·*m*CA, 139346-76-2; **1**·*p*CA, 139346-77-3; **1**·2*o*DM, 139346-80-8; **1**·2*m*DM, 139346-81-9; **1**·*p*DM, 139346-82-0; **1**·durene, 139346-88-6; **1**·PDE, 139346-89-7; **1**·ETB, 139346-90-0; dihydro-**1**, 139313-75-0; **2**, 114041-88-2; $2^{\cdot-}$·$EtNMe_3^+$, 139346-67-1; **2**·*p*X, 139346-74-0; **2**·*p*CA, 139346-78-4; **2**·*p*MA, 139346-79-5; **2**·2*o*DM, 139346-83-1; **2**·2*m*DM, 139346-84-2; **2**·*p*DM, 139346-85-3; **3**, 114041-89-3; **3**·2*m*DM, 139346-86-4; **3**·*p*DM, 139346-87-5; **5**, 83274-15-1; **6**, 114041-90-6; 7, 83274-16-2; **8**, 139346-91-1; **9**, 114041-91-7; **9** (Z = H), 35142-83-7; **10**, 139313-74-9; **11**, 114041-93-9; **13**, 139313-70-5; **14**, 41122-25-2; **14**·2,6-DMN, 139313-73-8; **15**, 109056-48-6; **15**·2,6-DMN, 139313-72-7; *o*DM, 91-16-7; *m*DM, 151-10-0; *p*DM, 150-78-7; *o*MA, 578-58-5; *m*MA, 100-84-5; *p*MA, 104-93-8; *o*CA, 766-51-8; *m*CA, 2845-89-8; *p*CA, 623-12-1; *o*X, 95-47-6; *m*X, 108-38-3; *p*X, 106-42-3; ETB, 100-41-4; 2,6-DMN, 581-42-0; 2,7-DMN, 582-16-1; 1,3-DMN, 575-41-7; 1,7-DMN, 575-37-1; PDE, 122-95-2; ClC_6H_4-*m*-Me, 108-41-8; ClC_6H_4-*p*-Me, 95-49-8; $TeCl_4$, 10026-07-0; durene, 95-93-2; malononitrile, 109-77-3; selenium oxychloride, 7791-23-3; *p*-chlorotoluene, 106-43-4.

Supplementary Material Available: Details of X-ray structural analyses, listings of atomic and thermal parameters and bond distances and angles, and thermal ellipsoids with atom numbering systems for **1**, **2**, **3**, $EtNMe_3^+2^{\cdot-}$, **13**, pX·**1**, 2,6-DMN·**1**, 2,7-DMN·**1**, pMA·**1**, and oMA·**1**, listing of CN stretching frequencies and analytical values for CT crystals of **1–3**, and listing of decomposition points, CN stretching frequencies, molar ratios, and electrical resistivities of CT crystals and anion radical salts of **2** (38 pages); listing of observed and calculated structure factors (47 pages). Ordering information is given on any current masthead page.

(32) Jia-xing, Y. *Acta Crystallogr. Sect. A* **1981**, *37*, 642; **1983**, *39*, 35.
(33) Sakurai, T.; Kobayashi, K. *Rikagaku Kenkyusho Hokoku* **1979**, *55*, 69.
(34) Klug, A. *Nature (London)* **1947**, *160*, 570.
(35) The conductivity measurement was carried out by Dr. Hideki Yamochi and Prof. Gunzi Saito at the Institute for Solid State Physics, The University of Tokyo.